ACS OMEGA
http://pubs.acs.org/journal/acsodf
Article

Magnesium-Catalyzed Dye-Embedded Polylactide Nanoparticles for the Effective Killing of Highly Metastatic B16F10 Melanoma Cells

Shweta Sagar,[§] Monika Pebam,[§] Rituparna Sinha, Aravind K. Rengan,* and Tarun K. Panda*

Cite This: *ACS Omega* 2024, 9, 14860−14866
Read Online

ABSTRACT: In the current research, dye-embedded polylactic acid (PLA) conjugate materials were synthesized using one-pot ring-opening polymerization (ROP), i.e., ($dtHP_{LA}$) (2-[(2,4,6-trimethylphenyl) imino]-1(2*H*)-acenaphthylenone-reduced-PLA) and ($dmHP_{LA}$) (monoiminoacenaphtheneone-reduced-PLA), and then, nanoparticles (NPs) were engineered in the size range of 150 ± 30 nm. P($dtHP_{LA}$) NPs were employed in the treatment of melanoma, an aggressive type of skin cancer, which mandates the development of novel techniques to enhance healing outcomes and eliminate adverse effects related to existing treatments. In addition to exhibiting strong intracellular absorption in the spheroid model, the P($dtHP_{LA}$) NPs exhibited a strong cytotoxic effect on B16F10 cells, which resulted in oxidative stress from the generation of reactive oxygen species (ROS) and cell death. Additionally, a live/dead experiment using P($dtHP_{LA}$) NPs revealed a notable reduction in cell viability.

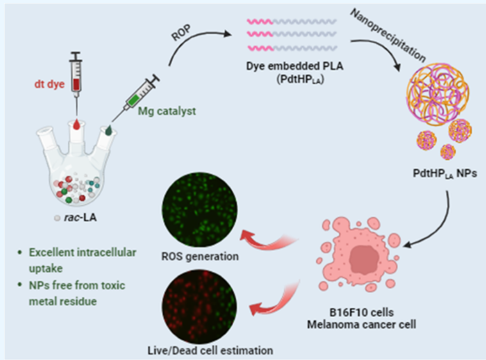

■ INTRODUCTION

Cancer is a devastating disease, and unilateral treatment approaches like chemotherapy and radiation therapy are employed as primary defense lines to protect from tumor heterogeneity. Out of several types, melanoma skin cancer accounts for the fifth most aggressive form, with a high mortality rate and metastatic condition.[1] High risk factors for skin cancer are ultraviolet exposure, genetic alteration, and fair skin; however, after following conventional treatment, patients suffer multidrug resistance (MDR), which prohibits cancer cells from amassing enough drugs, culminating in therapeutic failure and tumor relapses. In addition, it also causes serious side effects to the patient.[2,3] Therapeutic drugs are generally hydrophobic, small organic molecules, which leads to poor drug solubility. Nanomedical technology has emerged as a boon and has enhanced techniques for bioimaging and disease therapy, helping overcome the drawbacks of the selectivity of targeting cancerous cells by enabling the preferential delivery of medications to tumors. It provides an advanced mechanism of specific drug delivery to the targeted site due to the enhanced permeability and retention (EPR) effect.[3] Nanoparticles (NPs) attract attention as they have good bioavailability, systemic circulation, clearance, and bioimaging properties.[4] Nanosized drugs accumulate within the tumor region due to the EPR effect, which triggers the release of the specific drug. Due to cancer recurrence after undergoing treatment with adverse side effects,[5] NPs such as polymers, micelles, liposomes, metallic carbon, and gold-based nanoparticles were commonly used for theranostics approaches. However, literature reports state that metallic nanoparticles, due to their small size, suffer from toxicity, facing challenges in renal clearance. Therefore, the current study prefers a polymer nanosystem that has quick renal clearance and is biodegradable.

One of the tough challenges is the search for innovative delivery strategies that administer nanoparticles that reduce the side effects of conventional therapy.[6] One of the most well-known systems is targeted drug delivery, which reduces the negative effects of medicines by administering them directly to the tumor region.[6] Researchers who study drug delivery systems focus on the injection and packaging of drugs (as a micelle or nanoparticle) to prevent deterioration before they reach their target place in the body. Polymeric nanoparticles (PNPs) based on aliphatic polyesters, one of the several platforms created, are one of the environmentally friendly options. In recent years, a wide range of polymeric platforms have been created using a variety of structural types, such as micelles,[7−9] dendrimers,[10] hydrogels,[11] and encapsulant particles.[12−14] Drug delivery techniques utilizing biodegradable polymers like polyglycolic acid (PGA) and polylactic acid (PLA) have been documented in the literature.[15] Hence, biopolymers are an appropriate material to use for the safe and controlled delivery of medicinal drugs into cancer cells. Hydrophobic polymers are coprecipitated to create polymeric

Received: October 10, 2023
Revised: February 12, 2024
Accepted: March 12, 2024
Published: March 25, 2024

https://doi.org/10.1021/acsomega.3c07898
ACS Omega 2024, 9, 14860−14866

NPs, which provide precise medication release control. Drug distribution is made safe using NPs, which aid in the attachment of numerous agents and guard against enzyme-induced drug degradation.[16] Yet, when employed in vivo, these NPs have low drug loadings and weak encapsulation efficiencies.[17] PLAs are prominent polymers and are widely employed owing to their biodegradability and lack of toxicity. Tin(II) octoate [$Sn(Oct)_2$] is greatly used for PLA synthesis due to its high efficiency, superior solubility, and industrial use for the ring-opening polymerization (ROP) of lactones.[18] However, there are some concerns about the polymer's viability to be employed in food and medical packaging due to the probable buildup of tin residues in it.[19,20] Hence, there has been a huge drive to use less harmful organometal compounds that can exhibit equivalent or better performance characteristics. Although there are numerous known catalysts, group 2 metal catalysts have recently garnered interest due to their enhanced compatibility with biological systems. While magnesium is one of the most common metals on earth relative to other metals in the series, its reactivity in the ROP process has not received as much attention. It is intriguing to examine its reactivity due to its nontoxicity and necessity in our cells' regular metabolism. Even if there is a small amount of metal residue in the final polymer, it does not pose a threat in biological applications. Typically, D- or L-lactide polymers that have been specially purchased from companies are the polymers used. However, our goal was to examine the stereocomplex polymer formed by *rac*-LA ROP in drug delivery applications. Due to the strong intermolecular interaction between the L- and D-lactyl units, the stereocomplex (*sc*) polymer's synthesis offers a special way to improve the material's qualities. We continued to investigate the effectiveness of *sc*-PLA as a drug carrier through the encapsulation of medicines because of the material's superior mechanical and physical robustness. For tracking the drug molecules in vivo and monitoring their delivery and release in real time, one needs a fluorescent material with the drug. One approach is to incorporate fluorescent dyes or nanoparticles into the drug delivery system.[21,22] Compared to small molecule/polymer blend formulations, the preparation of polymer-linked materials entails a time-consuming, multistep organic synthesis. However, long-term applications, where side effects like "burst" release are essentially eliminated, benefit from the greater stability or regulated release of macromolecular compounds. Due to their ability to polymerize via ring-opening conjugation with PLA molecules, phenolic dyes play a significant role in this field. Even though covalent encapsulation techniques have several theoretical benefits, including high stability (no burst release), loading effectiveness, and predictable drug release, their development is frequently stymied by low yields and complicated synthetic schemes that call for multiple protection/deprotection steps.

Here, we demonstrate the synthesis of unique nanoparticles involving a well-known organic dye combined with PLA for the treatment of melanoma cancer (Figure 1). The polymers were made via a single-pot reaction using a magnesium organometallic catalyst and *rac*-LA via ROP. We were able to demonstrate that this approach has several advantages over conventional encapsulation techniques, including the ability to increase drug delivery to melanoma cancer cells. The prepared $dmHP_{LA}$ (monoiminoacenaphtheneone-reduced-PLA) and $dtHP_{LA}$ (2-[(2,4,6-trimethylphenyl) imino]-1(2*H*)-acenaphthylenone-reduced-PLA) NPs' mode of administration will be through topical administration, a noninvasive route, that has several advantages that can target passive targeting. Nanocarriers increase the drug solubility, which is poorly water-soluble, further reducing skin irritation via avoiding direct contact on the skin surface. Moreover, polymeric nanoparticles have shown sustained drug release in the tumor microenvironment when applied topically.

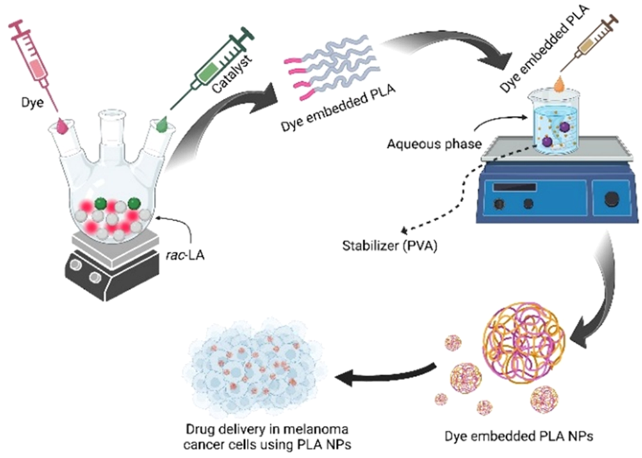

Figure 1. Schematic representation of the synthesis of dye-embedded PLA NPs and their application in cancer drug delivery.

RESULTS AND DISCUSSION

Dye-embedded PLA polymer conjugate was synthesized using reduced organic dyes such as (2,6-diisopropylphenyl imino)-acenaphthenone (dpp-mian) and (2,4,6-trimethylphenyl imino) acenaphthenone (dpp-tpian) through the ROP procedure as shown in Scheme 1. A magnesium catalyst, previously reported in our group, was used for the ROP reaction at very mild conditions in the toluene solvent.[23] The polymer was quenched finally by acidic methanol and recrystallized with dichloromethane and hexane to yield an orange color for dpp-mian ($dmHP_{LA}$) and a green color for dpp-tpian ($dtHP_{LA}$) compounds, respectively. They are well-characterized by ^1H and ^{13}C NMR spectroscopies. The absence of a hydroxyl group in the ^1H NMR of $dmHP_{LA}$ clearly shows that the conjugation is through the oxygen atom and the carbonyl carbon of the PLA chain (Figure S7). Gel permeation chromatography (GPC) analysis reveals the monomodal peak, indicating the successful synthesis of a well-controlled molecular weight polymer (M_w = 20.2, 24.6 *k*Da; PDI = 1.2, 1.1 for $dmHP_{LA}$ and $dtHP_{LA}$, respectively) (Figure S9).

Furthermore, the probability of meso links, which is indicated by the parameter P_m, was estimated to investigate the stereoregularity of the resultant PLA materials. This probability may be obtained from the homonuclear decoupled ^1H NMR spectra by integrating the relative tetrad intensities (Figure 2).[24] Both the PLA sample recorded spectra demonstrate an intense signal in the methine region that can be attributed to the mmm tetrad, indicating stereoselective polymerization and the development of PLA with a substantial amount of isotacticity. These ^1H NMR characteristics indicate the formation of stereomultiblock PLA with P_m values of 0.78 and 0.83 for $dmHP_{LA}$ and $dtHP_{LA}$, respectively. The higher P_m value can be ascribed to the decreasing bulkiness from the (2,6-diisopropylphenyl) aniline to the (2,4,6-trimethyl) aniline. The thermal characteristics of the polymers (glass-transition

https://doi.org/10.1021/acsomega.3c07898
ACS Omega 2024, 9, 14860−14866

Scheme 1. Synthesis of dpp-mian/tpian-H-PLA (dm/t-H-P_{LA})

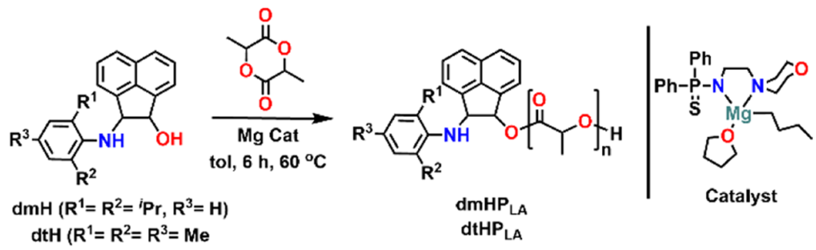

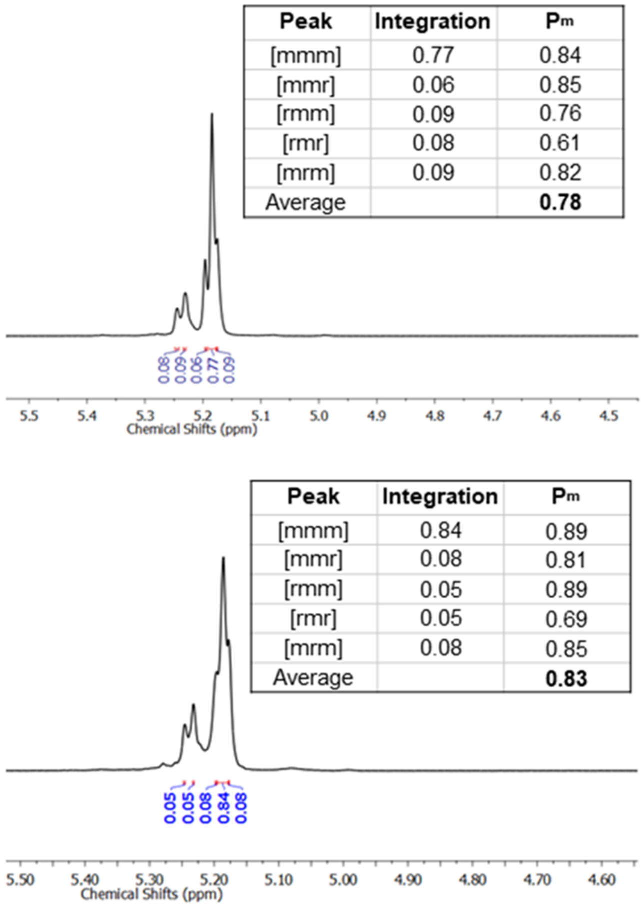

Peak	Integration	Pm
[mmm]	0.77	0.84
[mmr]	0.06	0.85
[rmm]	0.09	0.76
[rmr]	0.08	0.61
[mrm]	0.09	0.82
Average		**0.78**

Peak	Integration	Pm
[mmm]	0.84	0.89
[mmr]	0.08	0.81
[rmm]	0.05	0.89
[rmr]	0.05	0.69
[mrm]	0.08	0.85
Average		**0.83**

Figure 2. $^1H\{^1H\}$ NMR spectra of methine regions for PLA chains: (A) $dmHP_{LA}$ and (B) $dtHP_{LA}$.

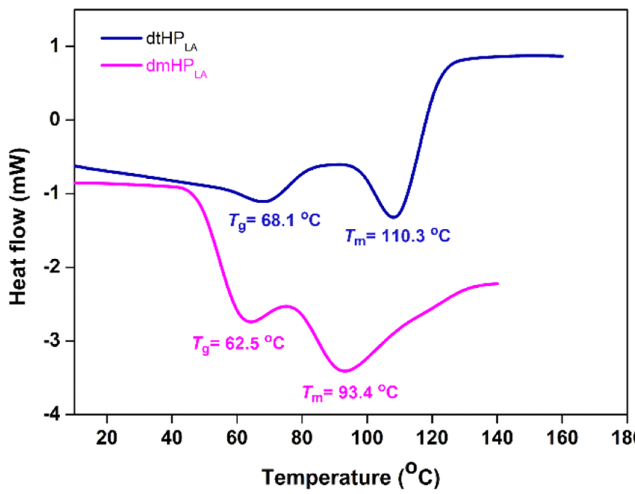

Figure 3. DSC thermograms of $dmHP_{LA}$ and $dtHP_{LA}$.

temperature T_g, melting temperature T_m) were determined by using differential scanning calorimetry (DSC), which further demonstrates the high isotacticity of the polymers. The PLA adducts showed high melting points (T_m) at 93.4 and 110.3 °C for $dmHP_{LA}$ and $dtHP_{LA}$, respectively (Figure 3).

After the successful synthesis of dye-PLA adducts, the compounds were utilized in the synthesis of their NPs. We developed P(dm/t-HP_{LA}) NPs to understand their role in bioimaging as well as for bioefficacy studies against the melanoma cell line B16F10. P(dm/t-HP_{LA}) NPs have a size range of 258.8 ± 30.5 nm in hydrodynamic diameter, and they show a spherical shape when observed using TEM between 150 ± 30 nm. The polydispersity indexes (PDIs) of P($dmHP_{LA}$) NPs and P($dtHP_{LA}$) NPs were 0.295 and 0.093, respectively, through DLS. The ζ-potentials of P($dmHP_{LA}$) NPs and P($dtHP_{LA}$) NPs were −1.04 ± 2.26 and −3.23 ± 0.53 mV, respectively. TEM image analysis revealed that the formed NPs are spherical with a size range of 150 ± 30 nm. The size difference between DLS and TEM was due to different working principles as DLS is based on light-scattering hydrodynamic data, which can be easily influenced by particle agglomeration.[25] On the contrary, TEM imaging analysis was performed after the sample was dried completely, resulting in a smaller size. These findings corroborate TEM with DLS data (Figure 4). They have selective targeted delivery against melanoma cancer and selective toxicity, as well as excellent intracellular uptake, as demonstrated in 2D and 3D models.

Different pH buffers of 5.8 and 7.4 were used for incubating at 37 °C as we could understand the release profile of the NPs formed in acidic conditions. Here, pH 5.8 showed more drug release within a short period of time in comparison to normal physiological pH 7.4. High acidification of the tumor microenvironment is attributed to hypoxia or lack of oxygen supply owing to inadequate blood flow in the tumor region.[26] The amount of drug release at 9 h at pH 5.8 was found to be higher (75.42 ± 2.41% of the dtH present in P(dtHPLA) NPs and 42.43 ± 8.17% of the dmH present in P(dmHPLA) NPs) compared to that at pH 7.4 (76.05 ± 7.2% of the dtH present in P($dtHP_{LA}$) NPs and 24.39 ± 5.78% of the dmH present in P($dmHP_{LA}$) NPs). The P(dtHPLA) NPs showed a higher absorption value in acidic pH values 5.8 and 7.4 when compared to the absorption value present in P(dmHPLA) NPs. Overall, P(dtHPLA) NPs can be a novel therapeutic agent because the PLA present in the nanoparticle is free from tin(II), being replaced with Mg, which helps increase the encapsulation efficiency of dmH compounds and in site-specific drug delivery for cancer theranostics.[27−30] The NPs containing Mg showed excellent biocompatibility and stability and low IC50 values in comparison to copper, manganese, tin, and cobalt nanoparticles. Mg-based nanocomposites like MnO

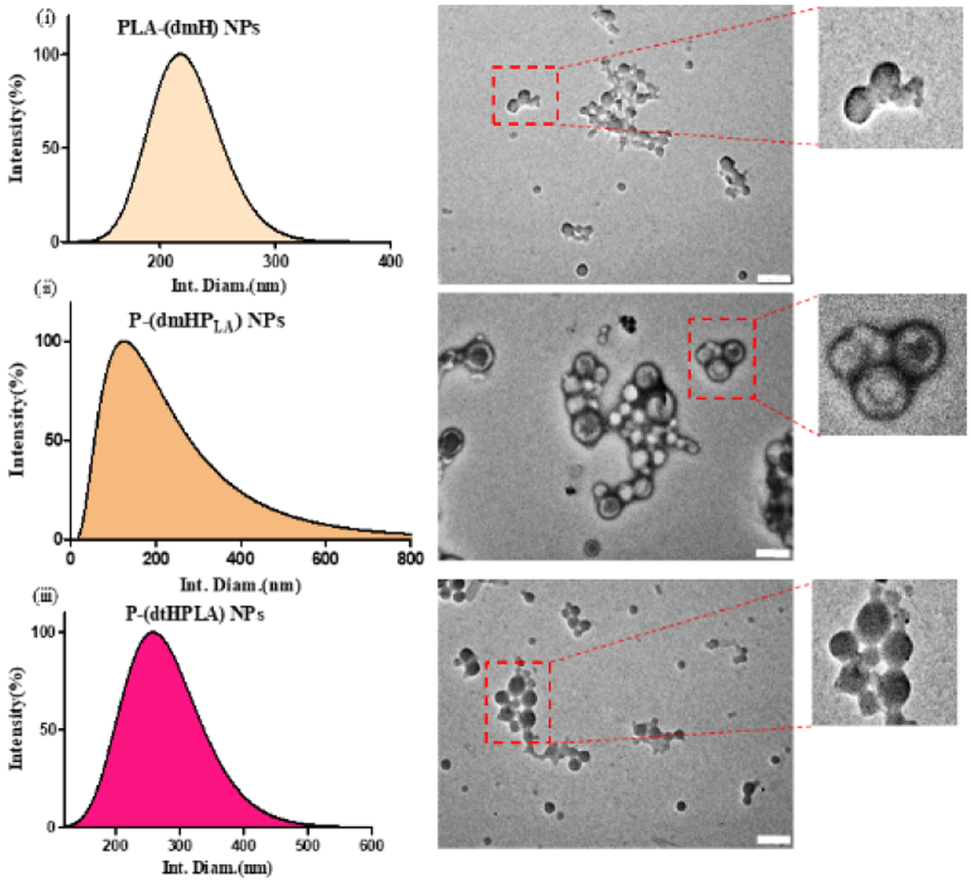

Figure 4. DLS and TEM analysis of (i) PLA-(dmH) NPs (ii) P(dmHP$_{LA}$) NPs and (iii) P(dtHP$_{LA}$) NPs respectively (scale bar: 500 μm).

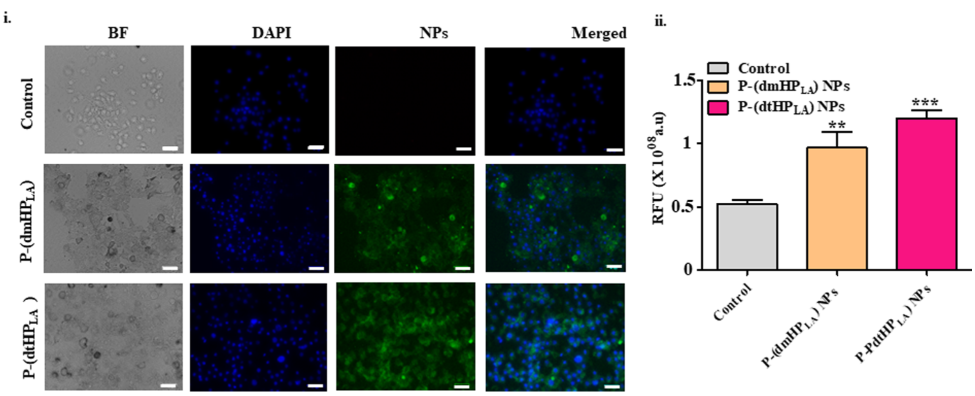

Figure 5. (i) Intracellular uptake and (ii) qualitative analysis of P(dmHP$_{LA}$) NPs and P(dtHP$_{LA}$) NPs in B16F10 cells in a 2D model after 12 h of incubation (scale bar: 50 μm).

with the surface modified with long hydrocarbon chains exhibited high optical properties and encapsulation efficiency (transmittance: 94.9%).[31−33] The developed NPs, consisting of P(dmHP$_{LA}$) NPs and P(dtHP$_{LA}$) NPs, were synthesized by the solvent emulsification method with slight modifications. They were then subjected to UV−vis spectroscopy, giving peaks at 303 and 306 nm, respectively. To understand the shape, size, and morphology of the synthesized NPs, DLS analysis along with TEM imaging was performed. The hydrodynamic size analysis of the NPs was exhibited using DLS measurements, respectively, as 256 ± 45.1 and 258.8 ± 30.5 nm. TEM image analysis revealed that the formed NPs are spherical with a size range of 150 ± 30 nm. These findings corroborate the DLS data (Figure 4).

To understand the intracellular uptake of P(dmHP$_{LA}$) NPs and P(dtHP$_{LA}$) NPs, the intracellular uptake assay was performed using B16F10 cells, wherein the NPs were incubated for 12−16 h, and interestingly, it was found that P(dtHP$_{LA}$) NPs showed a high green fluorescence intensity when compared to P(dmHP$_{LA}$) NPs (Figure 5). Both qualitative and quantitative data were analyzed by observing the intracellular uptake in vitro and in 3D spheroid models. Intracellular uptake studies are a crucial step in determining whether the PLA NPs, i.e., P(dtHP$_{LA}$) NPs, have been retained within the tumor microenvironment. We have observed that due to the presence of more electron-donating groups to the phenyl ring in (2,4,6-trimethylphenyl) amine, the richness of P(dtHPLA) NPs in intracellular uptake was observed. The

https://doi.org/10.1021/acsomega.3c07898
ACS Omega 2024, 9, 14860−14866

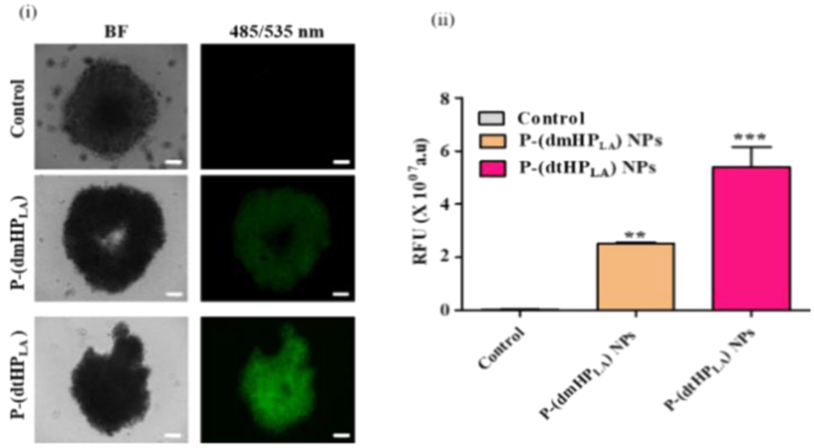

Figure 6. (i) Intracellular uptake and (ii) qualitative analysis of P(dmHP$_{LA}$) NPs and P(dtHP$_{LA}$) NPs in B16F10 cells in a 3D model after 12 h of incubation (scale bar: 100 μm).

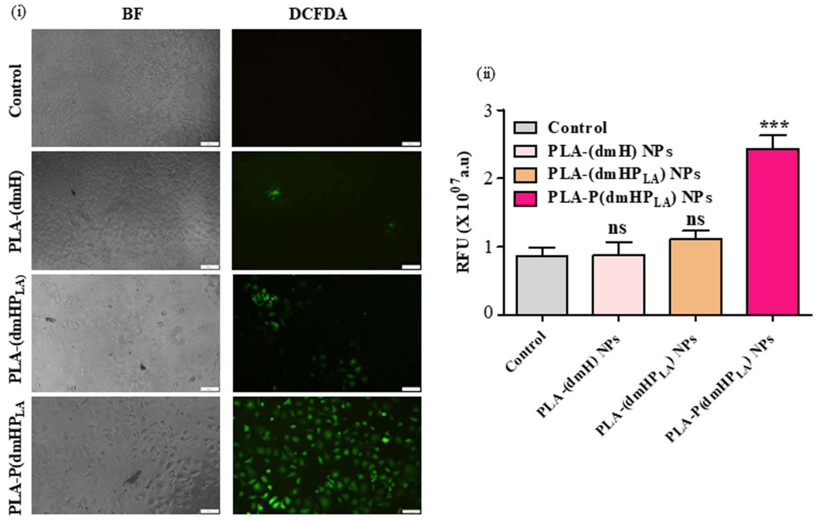

Figure 7. ROS generation assay estimation using DCFDA analysis in B16F10 cells. The concentration used was 15 μg/mL (scale bar: 100 μm).

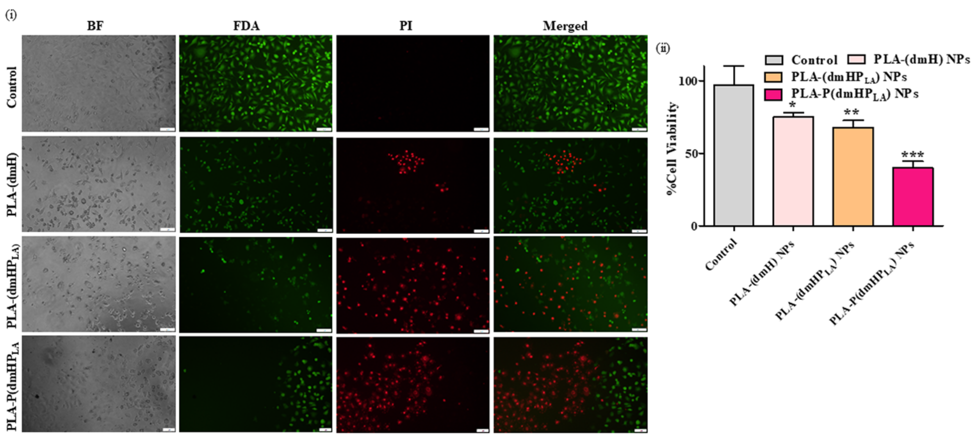

Figure 8. Live/dead cell estimation assay using FDA/PI staining representing (i) qualitatively and (ii) quantitatively (scale bar: 100 μm).

spheroid model was introduced to mimic the in vivo model that enhances intracellular uptake. The spheroid model helps in determining the penetration of NPs in the core region of the cells,[34,35] which correlates with the quantitative data represented in Figure 5. We observed a better cellular uptake of P(dtHP$_{LA}$) NPs in comparison to P(dmHP$_{LA}$) NPs inside the tumor volume of 3D spheroids (B16F10); it is confirmed that NPs diffuse inside the spheroids due to deep penetration and adherence.[35] These findings suggest that P(dtHP$_{LA}$)-inspired NPs help in bioimaging besides having anticancer properties.

https://doi.org/10.1021/acsomega.3c07898
ACS Omega 2024, 9, 14860−14866

The biocompatibility assay was performed in L929 and NIH 3T3 cells using PLA, the carrier agent. Cells were treated with different concentrations ranging from 1 to 10 μg/mL, and an MTT assay was performed (Figure S10). The carrier agent PLA has excellent biocompatibility. Reactive oxygen species (ROS) generation is an early diagnostic marker of cancer treatment. Polymer nanoparticles caused cytotoxic effects, thereby releasing ROS to highly malignant tumor cells. ROS generation leads to intracellular oxidative stress that overwhelms the redox adaptation, alters cellular stress, and causes cancer-specific cell death.[36] The effect of NPs on intracellular ROS was determined using B16F10 cells. The DCFDA assay helped in understanding the efficient ROS production when B16F10 cells were treated with P(dmHP$_{LA}$) NPs as compared to P(dtHP$_{LA}$) NPs and untreated (control) groups. These findings suggest that P(dtHP$_{LA}$) NPs promote significant ROS production that disturbs the redox balance, causing oxidative stress that leads to cell death. So the P(dtHP$_{LA}$) NP may be a potent anticancer candidate that has more bioavailability, having minimal cell damage to nearby tissues as it has significant ROS generation, causing cellular damage in the acidic tumor microenvironment.[37]

Further, to assess the cell death, the FDA/PI assay was performed by treating the B16F10 cells with 15 μg/mL concentration of NPs (Figures 6 and 7). Significant cell death was observed with the treatment performed with P(dtHP$_{LA}$) NPs when compared to other treatment groups of P(dmHP$_{LA}$) NPs. It correlates with the quantitative data owing to PI stains showing red fluorescence compared with the other control groups. The cell death mechanism of B16F10 might be induced due to the ability of P(dtHP$_{LA}$) NPs to penetrate the skin cancer region, thereby enhancing significant cell death.[38] In other words, it reflects the diminishing cell viability and cell count when treated with P(dtHP$_{LA}$) NPs, indicating a promising therapeutic agent (Figure 8).

CONCLUSIONS

In conclusion, this study reports the synthesis of a dye conjugated with PLA catalyzed by a magnesium initiator via ROP. We have developed respective P(dm/t-HP$_{LA}$) NPs to understand their role in bioimaging as well as for bioefficacy studies against the melanoma cell line B16F10, which implicates their route of administration through the transdermal route. P(dtHP$_{LA}$) NPs have a size range of 258.8 ± 30.5 nm in hydrodynamic diameter and shows a spherical shape when observed using TEM between 150 ± 30 nm. Furthermore, it showed selective targeted delivery against melanoma cancer and selective toxicity, as well as excellent intracellular uptake, as demonstrated in 2D and 3D models. These biodegradable P(dtHP$_{LA}$) NPs can be a novel therapeutic agent because the PLA present in the nanoparticle is free from tin(II), being replaced with Mg, which helped in increasing the encapsulation efficiency of dmH/dtH compounds as well as in site-specific drug delivery for cancer theranostics.

ASSOCIATED CONTENT

Supporting Information

The Supporting Information is available free of charge at https://pubs.acs.org/doi/10.1021/acsomega.3c07898.

Materials and methods; general considerations; synthesis; and characterization methods (PDF)

AUTHOR INFORMATION

Corresponding Authors

Aravind K. Rengan − *Department of Biomedical Engineering, Indian Institute of Technology Hyderabad, Kandi 502284 Telangana, India;* orcid.org/0000-0003-3994-6760; Email: aravind@bme.iith.ac.in

Tarun K. Panda − *Department of Chemistry, Indian Institute of Technology Hyderabad, Kandi 502284 Telangana, India;* orcid.org/0000-0003-0975-0118; Email: tpanda@chy.iith.ac.in, tpanda@iith.ac.in

Authors

Shweta Sagar − *Department of Chemistry, Indian Institute of Technology Hyderabad, Kandi 502284 Telangana, India;* orcid.org/0000-0001-6785-0585

Monika Pebam − *Department of Biomedical Engineering, Indian Institute of Technology Hyderabad, Kandi 502284 Telangana, India*

Rituparna Sinha − *Department of Chemistry, Indian Institute of Technology Hyderabad, Kandi 502284 Telangana, India*

Complete contact information is available at: https://pubs.acs.org/10.1021/acsomega.3c07898

Author Contributions

[§]S.S. and M.P. contributed equally. All authors have approved the final version of the manuscript.

Notes

The authors declare no competing financial interest.

ACKNOWLEDGMENTS

The authors appreciate the financial support received from the Science and Engineering Research Board (SERB), India, under Project No. CRG/2022/001941, ICMR (35/1/2020/GIA/Nano/BMS). The schematic and the graphical abstract were designed using biorender.com. S.S. and M.P. want to acknowledge their Prime Minister Research Fellowship ID No. 2000829 and the DST-INSPIRE fellowship IF180306, respectively.

REFERENCES

(1) Bastian, B. C. The Molecular Pathology of Melanoma: An Integrated Taxonomy of Melanocytic Neoplasia. *Annu. Rev. Pathol.: Mech. Dis.* **2014**, *9*, 239−271.

(2) Shapira, A.; Livney, Y. D.; Broxterman, H. J.; Assaraf, Y. G. Nanomedicine for Targeted Cancer Therapy: Towards the Overcoming of Drug Resistance. *Drug Resist. Updates* **2011**, *14* (3), 150−163.

(3) Song, Y.; Xie, Y.; Yang, J.; Li, R.; Jin, X.; Yang, J. A Poly(Ascorbyl Acrylate)-Containing Nanoplatform with Anticancer Activity and the Sequential Combination Therapy with Its Loaded Paclitaxel. *J. Mater. Chem. B* **2016**, *4* (40), 6588−6596.

(4) Yue, Z.; You, Z.; Yang, Q.; Lv, P.; Yue, H.; Wang, B.; Ni, D.; Su, Z.; Wei, W.; Ma, G. Molecular Structure Matters: PEG-b-PLA Nanoparticles with Hydrophilicity and Deformability Demonstrate Their Advantages for High-Performance Delivery of Anti-Cancer Drugs. *J. Mater. Chem. B* **2013**, *1* (26), 3239−3247.

(5) Cassano, R.; Cuconato, M.; Calviello, G.; Serini, S.; Trombino, S. Recent Advances in Nanotechnology for the Treatment of Melanoma. *Molecules* **2021**, *26* (4), No. 785, DOI: 10.3390/molecules26040785.

(6) Alvarez-Lorenzo, C.; Concheiro, A. Intelligent Drug Delivery Systems: Polymeric Micelles and Hydrogels. *Mini Rev. Med. Chem.* **2008**, *8*, 1065−1074, DOI: 10.2174/138955708785909952.

(7) Torchilin, V. P. Structure and Design of Polymeric Surfactant-Based Drug Delivery Systems. *J. Controlled Release* **2001**, *73*, 137−172, DOI: 10.1016/s0168-3659(01)00299-1.
(8) Gillies, E. R.; Fréchet, J. M. J. A New Approach towards Acid Sensitive Copolymer Micelles for Drug Delivery. *Chem. Commun.* **2003**, *3* (14), 1640−1641.
(9) Kim, S. H.; Tan, J. P. K.; Nederberg, F.; Fukushima, K.; Colson, J.; Yang, C.; Nelson, A.; Yang, Y. Y.; Hedrick, J. L. Hydrogen Bonding-Enhanced Micelle Assemblies for Drug Delivery. *Biomaterials* **2010**, *31* (31), 8063−8071.
(10) Mintzer, M. A.; Grinstaff, M. W. Biomedical Applications of Dendrimers: A Tutorial. *Chem. Soc. Rev.* **2011**, *40* (1), 173−190.
(11) Qiu, Y.; Park, K. Environment-Sensitive Hydrogels for Drug Delivery. *Adv. Drug Delivery Rev.* **2001**, *53*, 321−339, DOI: 10.1016/s0169-409x(01)00203-4.
(12) Yu, X.; Pishko, M. V. Nanoparticle-Based Biocompatible and Targeted Drug Delivery: Characterization and in Vitro Studies. *Biomacromolecules* **2011**, *12* (9), 3205−3212.
(13) Yan, Y.; Such, G. K.; Johnston, A. P. R.; Lomas, H.; Caruso, F. Toward Therapeutic Delivery with Layer-by-Layer Engineered Particles. *ACS Nano* **2011**, *5*, 4252−4257.
(14) Sankaranarayanan, J.; Mahmoud, E. A.; Kim, G.; Morachis, J. M.; Almutairi, A. Multiresponse Strategies to Modulate Burst Degradation and Release from Nanoparticles. *ACS Nano* **2010**, *4* (10), 5930−5936.
(15) Sinha, V. R.; Khosla, L. Bioabsorbable Polymers for Implantable Therapeutic Systems. *Drug Dev. Ind. Pharmacy* **1998**, *24*, 1129−1138, DOI: 10.3109/03639049809108572.
(16) Tong, R.; Cheng, J. Controlled Synthesis of Camptothecin-Polylactide Conjugates and Nanoconjugates. *Bioconjugate Chem.* **2010**, *21* (1), 111−121.
(17) Cheng, J.; Teply, B. A.; Sherifi, I.; Sung, J.; Luther, G.; Gu, F. X.; Levy-Nissenbaum, E.; Radovic-Moreno, A. F.; Langer, R.; Farokhzad, O. C. Formulation of Functionalized PLGA-PEG Nanoparticles for in Vivo Targeted Drug Delivery. *Biomaterials* **2007**, *28* (5), 869−876.
(18) Sobczak, M.; Kolodziejski, W. Polymerization of Cyclic Esters Initiated by Carnitine and Tin (II) Octoate. *Molecules* **2009**, *14* (2), 621−632.
(19) Santulli, F.; Gravina, G.; Lamberti, M.; Tedesco, C.; Mazzeo, M. Zinc and Magnesium Catalysts for the Synthesis for PLA and Its Degradation: Clues for Catalyst Design. *Mol. Catal.* **2022**, *528*, 112480 DOI: 10.1016/j.mcat.2022.112480.
(20) Gadomska-Gajadhur, A.; Ruśkowski, P. Biocompatible Catalysts for Lactide Polymerization - Catalyst Activity, Racemization Effect, and Optimization of the Polymerization Based on Design of Experiments. *Org. Process Res. Dev.* **2020**, *24* (8), 1435−1442.
(21) Sitia, L.; Ferrari, R.; Violatto, M. B.; Talamini, L.; Dragoni, L.; Colombo, C.; Colombo, L.; Lupi, M.; Ubezio, P.; D'Incalci, M.; Morbidelli, M.; Salmona, M.; Moscatelli, D.; Bigini, P. Fate of PLA and PCL-Based Polymeric Nanocarriers in Cellular and Animal Models of Triple-Negative Breast Cancer. *Biomacromolecules* **2016**, *17* (3), 744−755.
(22) Reisch, A.; Klymchenko, A. S. Fluorescent Polymer Nanoparticles Based on Dyes: Seeking Brighter Tools for Bioimaging. *Small* **2016**, *12*, 1968−1992, DOI: 10.1002/smll.201503396.
(23) Sagar, S.; Bano, K.; Sarkar, A.; Pal, K.; Panda, T. K. Magnesium Promoted Active and Isoselective ROP of Rac-Lactide and ϵ-Caprolactone Under Mild Conditions. *Eur. J. Inorg. Chem.* **2022**, *2022* (34), No. e202200494, DOI: 10.1002/ejic.202200494.
(24) Coudane, J.; Ustariz-Peyret, C.; Schwach, G.; Vert, M. *More About the Stereodependence of DD and LL Pair Linkages During the Ring-Opening Polymerization of Racemic Lactide*; John Wiley & Sons, Inc., 1997; Vol. 35.
(25) Inam, W.; Bhadane, R.; Akpolat, R. N.; Taiseer, R. A.; Filippov, S. K.; Salo-Ahen, O. M. H.; Rosenholm, J. M.; Zhang, H. Interactions between Polymeric Nanoparticles and Different Buffers as Investigated by Zeta Potential Measurements and Molecular Dynamics Simulations. *View* **2022**, *3* (4), 20210009.
(26) Shafiei, G.; Jafari-Gharabaghlou, D.; Farhoudi-Sefidan-Jadid, M.; Alizadeh, E.; Fathi, M.; Zarghami, N. Targeted Delivery of Silibinin via Magnetic Niosomal Nanoparticles: Potential Application in Treatment of Colon Cancer Cells. *Front. Pharmacol.* **2023**, *14*, No. 1174120.
(27) Uppal, G.; Thakur, A.; Chauhan, A.; Bala, S. Magnesium Based Implants for Functional Bone Tissue Regeneration − A Review. *J. Magnesium Alloys* **2022**, *10*, 356−386, DOI: 10.1016/j.jma.2021.08.017.
(28) Ferrández-Montero, A.; Lieblich, M.; González-Carrasco, J. L.; Benavente, R.; Lorenzo, V.; Detsch, R.; Boccaccini, A. R.; Ferrari, B. Development of Biocompatible and Fully Bioabsorbable PLA/Mg Films for Tissue Regeneration Applications. *Acta Biomater.* **2019**, *98*, 114−124.
(29) Abdeljawad, M. B.; Carette, X.; Argentati, C.; Martino, S.; Gonon, M. F.; Odent, J.; Morena, F.; Mincheva, R.; Raquez, J. M. Interfacial Compatibilization into Pla/Mg Composites for Improved in Vitro Bioactivity and Stem Cell Adhesion. *Molecules* **2021**, *26* (19), No. 5944, DOI: 10.3390/molecules26195944.
(30) Argentati, C.; Dominici, F.; Morena, F.; Rallini, M.; Tortorella, I.; Ferrandez-Montero, A.; Pellegrino, R. M.; Ferrari, B.; Emiliani, C.; Lieblich, M.; Torre, L.; Martino, S.; Armentano, I. Thermal Treatment of Magnesium Particles in Polylactic Acid Polymer Films Elicits the Expression of Osteogenic Differentiation Markers and Lipidome Profile Remodeling in Human Adipose Stem Cells. *Int. J. Biol. Macromol.* **2022**, *223*, 684−701.
(31) Nejati, M.; Rostami, M.; Mirzaei, H.; Rahimi-Nasrabadi, M.; Vosoughifar, M.; Nasab, A. S.; Ganjali, M. R. Green Methods for the Preparation of MgO Nanomaterials and Their Drug Delivery, Anti-Cancer and Anti-Bacterial Potentials: A Review. *Inorg. Chem. Commun.* **2022**, *136*, No. 109107.
(32) Kim, M. S.; Jang, H.; Baek, S. D.; Yoon, S. Y.; Kim, S.; Lee, S.; Lee, J. H.; Song, J.; Myoung, J. M. Highly Dispersible Surface-Modified Magnesium Oxide Nanoparticle-Acrylate Nanocomposites as a Transparent OLED Encapsulation Material. *Prog. Org. Coat.* **2021**, *154*, 106196.
(33) Abinaya, S.; Kavitha, H. P. Magnesium Oxide Nanoparticles: Effective Antilarvicidal and Antibacterial Agents. *ACS Omega* **2023**, *8* (6), 5225−5233.
(34) Pebam, M.; Rajalakshmi, P. S.; Gangopadhyay, M.; Thatikonda, S.; Rengan, A. K. Terminalia Chebula Polyphenol and Near-Infrared Dye-Loaded Poly(Lactic Acid) Nanoparticles for Imaging and Photothermal Therapy of Cancer Cells. *ACS Appl. Bio Mater.* **2022**, *5* (11), 5333−5346.
(35) Ferreira, L. P.; Gaspar, V. M.; Monteiro, M. V.; Freitas, B.; Silva, N. J. O.; Mano, J. F. Screening of Dual Chemo-Photothermal Cellular Nanotherapies in Organotypic Breast Cancer 3D Spheroids. *J. Controlled Release* **2021**, *331*, 85−102.
(36) Perillo, B.; Di Donato, M.; Pezone, A.; Di Zazzo, E.; Giovannelli, P.; Galasso, G.; Castoria, G.; Migliaccio, A. ROS in Cancer Therapy: The Bright Side of the Moon. *Exp. Mol. Med.* **2020**, *52*, 192−203, DOI: 10.1038/s12276-020-0384-2.
(37) Lin, Y.; Jiang, M.; Chen, W.; Zhao, T.; Wei, Y. Cancer and ER Stress: Mutual Crosstalk between Autophagy, Oxidative Stress and Inflammatory Response. *Biomed. Pharmacother.* **2019**, *118*, No. 109249, DOI: 10.1016/j.biopha.2019.109249.
(38) Li, X. D.; Liang, X. L.; Yue, X. L.; Wang, J. R.; Li, C. H.; Deng, Z. J.; Jing, L. J.; Lin, L.; Qu, E. Z.; Wang, S. M.; Wu, C. L.; Wu, H. X.; Dai, Z. F. Imaging Guided Photothermal Therapy Using Iron Oxide Loaded Poly(Lactic Acid) Microcapsules Coated with Graphene Oxide. *J. Mater. Chem. B* **2014**, *2* (2), 217−223.